B cell class switch recombination is regulated by DYRK1A through MSH6 phosphorylation

Liat Stoler-Barak
Weizmann Institute of Science
Ethan Harris
Department of Hematology, St. Jude Children's Research Hospita
Ayelet Peres
https://orcid.org/0000-0002-0188-7315
Hadas Hezroni
Weizmann Institute of Science
Mirela Kuka
Division of Immunology, Transplantation and Infectious Diseases and Experimental Imaging Center
Amalie Grenov
weizmann institute https://orcid.org/0000-0001-6310-565X
Neta Gurwicz
Weizmann Institute
Meital Kupervaser
Weizmann Institute of Science
Bon Ham Yip
Department of Hematology, St. Jude Children's Research Hospital
Matteo Iannacone
San Raffaele Scientific Institute & University https://orcid.org/0000-0002-9370-2671
Gur Yaari
Faculty of Engineering
John Crispino
St Jude Children's Research Hospital https://orcid.org/0000-0002-8182-8306
Ziv Shulman (ziv.shulman@weizmann.ac.il)
Weizmann Institute of Science https://orcid.org/0000-0002-9604-212X

Article

Keywords:

Posted Date: July 5th, 2022

DOI: https://doi.org/10.21203/rs.3.rs-1779641/v1

B cell class switch recombination is regulated by DYRK1A through MSH6 phosphorylation

Liat Stoler-Barak[1], Ethan Harris[2], Ayelet Peres[3], Hadas Hezroni[1], Mirela Kuka[5], Amalie Grenov[1], Neta Gurwicz[1], Meital Kupervaser[4], Bon Ham Yip[2], Matteo Iannacone[5,6], Gur Yaari[3], John D. Crispino[2] and Ziv Shulman[1]

[1] Department of Immunology, Weizmann Institute of Science, Rehovot, Israel.
[2] Department of Hematology, St. Jude Children's Research Hospital, Memphis, TN, 38105, USA.
[3] Faculty of Engineering, Bar Ilan University, Ramat Gan 52900, Israel.
[4] De Botton Institute for Proteomics, Grand Israel National Center for Personalized Medicine, Weizmann Institute of Science, Rehovot, Israel.
[5] Vita-Salute San Raffaele University and Division of Immunology, Transplantation and Infectious Diseases, IRCCS San Raffaele Scientific Institute, Milan, Italy
[6] Experimental Imaging Center, IRCCS San Raffaele Scientific Institute, Milan, Italy

Abstract

Protection from viral infections depends on immunoglobulin isotype switching, which endows antibodies with effector functions. Here, we found that the protein kinase DYRK1A is essential for B cell-mediated protection from viral infection and effective vaccination through regulation of class switch recombination (CSR). *Dyrk1a*-deficient B cells were impaired in CSR activity in vivo and in vitro. Phosphoproteomic screens and kinase-activity assays identified MSH6, a DNA mismatch repair protein, as a direct substrate for DYRK1A, and deletion of a single phosphorylation site impaired CSR. After CSR and germinal center seeding, DYRK1A was required for proper clonal expansion of antigen-specific B cells through attenuation of proliferation. These findings reveal DYRK1A-mediated biological mechanisms of B cell immune responses that may be used for manipulation in antibody-mediated autoimmunity.

Introduction

Effective long-lasting protection from invading pathogens depends on the generation of antibodies by the infected host[1,2]. In addition, antibodies can play a role in the clearance of invading microbes in a primary immune response[3] through pathogen neutralization activity and induction of a range of cell-mediated effector functions[4–6]. These include NK-mediated killing of infected cells, and pathogen clearance by phagocytes through the interaction of the Fc part of the immunoglobulin with Fc-receptors that are expressed on immune cells[4,5,7]. Furthermore, the Fc-part of the antibody can activate the complement system, which involves a series of enzyme-mediated cleavage activities that can lead to killing of the target cells[8]. Similar antibody functions play a role in the clearance of aberrant self cells, such as malignant tumors,[6] and induce tissue damage in autoimmune diseases[5].

Antibody effector functions are determined by their isotype class. Prior to antigen encounters, naive B cells express both IgM and IgD B cell receptors (BCRs) on their surface[9,10]. Following cognate antigen interaction, and in response to mitogens and specific cytokines, B cells can switch their immunoglobulin isotype through a process known as class switch recombination (CSR)[11,12]. This mechanism involves the generation of nucleotide mismatches at the immunoglobulin switch regions by deamination of cytidine to uracil through activation-induced cytidine deaminase (AID) activity, generation of DNA breaks, and activation of DNA repair mechanisms[11,13–17].

Germinal centers are the major source of class-switched and long-lived plasma cells. These are microanatomical sites that are seeded by antigen-specific B cells about 5 days after pathogen infection or vaccination[9]. In these niches, B cells mutate their immunoglobulin genes followed by B cell receptors (BCR)-affinity-based selection for clonal expansion and differentiation into plasma cells (PCs)[18]. Within the GC, T follicular helper cells select B cells for clonal expansion through triggering CD40 and ICOSL activation on GC B cells and through cytokine secretion.

These signals increase the cell division rate of the selected clones through initial triggering of Myc transcription and downstream genetic programs within the GC light zone[19,20], followed by a transition into the GC dark zone, where rapid cell proliferation occurs[9,21,22].

DYRK family members are master regulators of proliferation in many cell types[23]. These enzymes are dual-specificity protein kinases that can autophosphorylate tyrosines, thereby activating their serine and threonine phosphorylation activity on target proteins[24,25]. Since the DYRK1A locus is located on a region of chromosome 21 that is duplicated in Down syndrome, it is the most extensively studied family member[26,27]. Phosphorylation of Myc, c-Jun, Cyclin D1 and Cyclin D3 by DYRK1A labels these proteins for proteasomal degradation, thereby attenuating the rate and magnitude of cell division[23,28–33]. Myc and many other DYRK1A targets are expressed in pre-GC B cells and in GC B cells that are selected for enhanced proliferation by cognate T cells[21,22]. Yet, although the DYRK1A is a master regulator of cell cycle progression, its role in rapidly proliferating GC B cells during an immune response was not examined, and it is not known whether other DYRK1A-mediated mechanisms contribute to the generation of protective antibodies and B cell clonal expansion.

Here, we examined the role of DYRK1A during the B cell immune response to viral infection and vaccine-derived antigens. We found that DYRK1A is essential for CSR, mediated through phosphorylation of MSH6. Furthermore, DYRK1A maintains robust clonal expansion of antigen-specific B cells in GCs through attenuation of cell cycle progression.

Results

Class-switch recombination requires DYRK1A independently of B cell proliferation

To study the role of DYRK1A in B cells, we crossed mice carrying a conditional inactivation of *Dyrk1a* gene with mice expressing B cell-specific Cre, under the CD23 promoter (*CD23.Cre.Dyrk1a*$^{fl/fl}$)[25,34]. B cells derived from littermate control mice (*CD23.Cre.Dyrk1a*$^{+/+}$) expressed DYRK1A, and its levels were increased in response to LPS stimulation[35], while B cells derived from *CD23.Cre.Dyrk1a*$^{fl/fl}$ mice lacked DYRK1A before and after stimulation with LPS **(Figure 1A)**. To examine whether DYRK1A plays a role in B cell activation and proliferation, splenic B cells were stimulated with LPS for 16 hours and CD86 upregulation, a hallmark of B cell activation, was examined. Flow cytometry analysis revealed that *Dyrk1a*-deficient and control B cells expressed similar levels of CD86 **(Figure 1B)**. Furthermore, B cell proliferation was examined through stimulation of cultured CellTrace Violet (CTV)-labeled cells with LPS or αIgM for 3 days. Although stimulation with αIgM resulted in decreased *Dyrk1a*-deficient B cell division and proliferation relative to WT, as measured by CTV dilution, stimulation with LPS showed a significant increase in those measurements **(Figure 1C)**. Furthermore, we directly investigated CSR in proliferating B cells by stimulation of splenic B cells with LPS in the presence of IL-4, followed by flow cytometry analysis after 3 days. Whereas a population of B cells that expressed IgG1 in response to the stimulation was detected in the control, *Dyrk1a*-deficient B cells did not show a similar increase in the frequency of IgG1-positive cells above the background of unstimulated controls **(Figure 1D)**. Of note, lack of effective proliferation could not account for the diminished CSR since *Dyrk1a*-deficient B cells that were stimulated with LPS. Thus, DYRK1A is required for CSR but not for B cell activation.

Figure 1

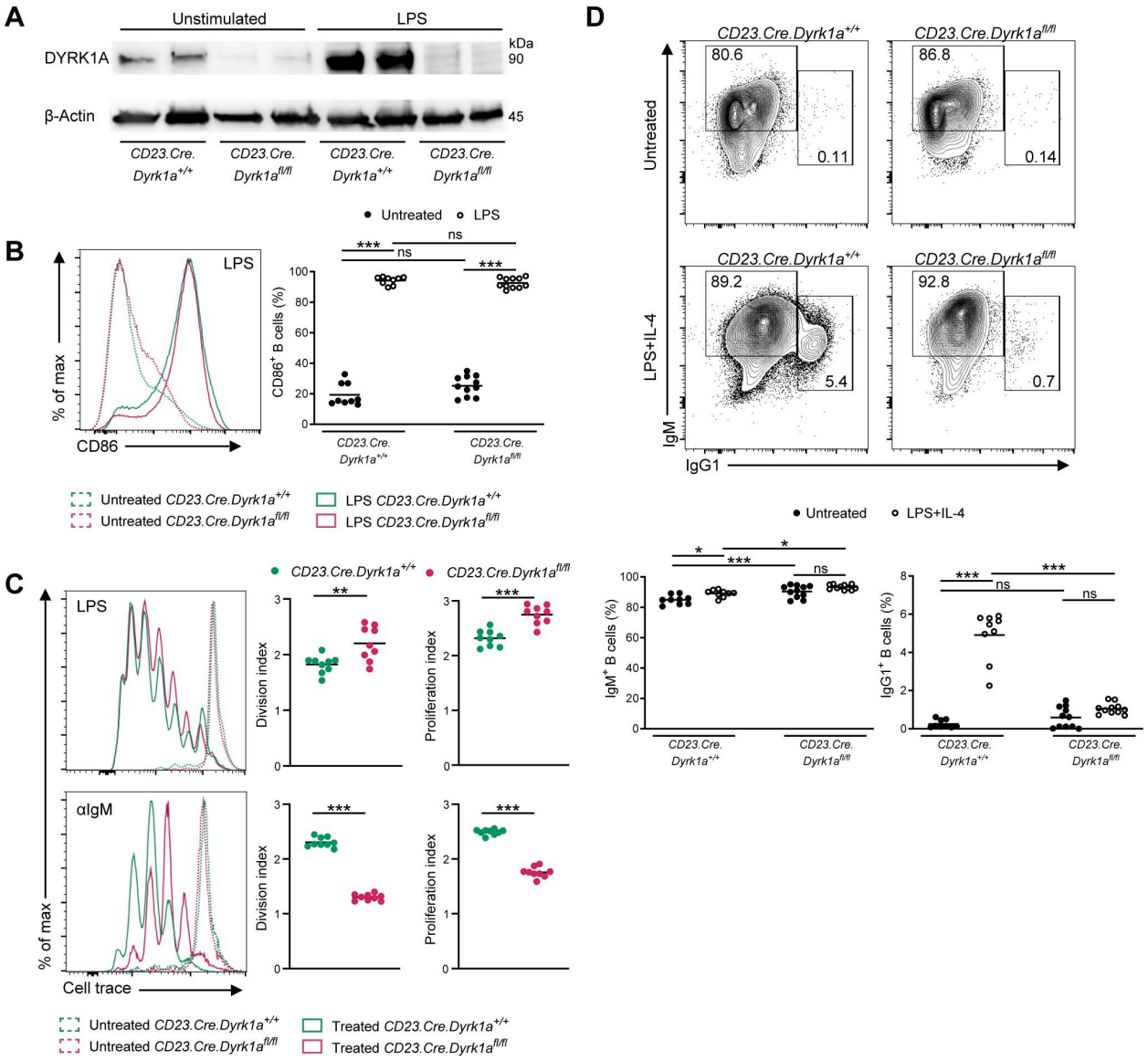

Figure 1. Class-switch recombination requires DYRK1A independently of B cell proliferation. (A) DYRK1A protein expression was determined by western blot analysis of B cells that were either left unmanipulated or stimulated with LPS for 3 days. Blots show two independent biological repeats. **(B)** Representative flow cytometry histograms and frequencies of activated B cells 16 hours after LPS stimulation in-vitro (n=9-11; three independent experiments, one-way ANOVA). **(C)** Representative flow cytometry histograms and quantification of CellTrace Violet dilutions representing the proliferation of splenic LPS-treated or αIgM B cells for 3 days. (n=9; three independent experiments, two-tailed Student's t-test). **(D)** Representative flow cytometry plots and frequencies of class-switched B cells derived from naive spleens that were either left unmanipulated or stimulated in-vitro with LPS + murine IL-4 for 3 days (n=9-11; three

independent experiments, one-way ANOVA). Each dot in the graphs represents a single mouse; * P=0.05, ** P≤0.01, ***P≤0.001, ns, not significant.

MSH6 is a direct target of DYRK1A phosphorylation

To further explore the mechanism of DYRK1A-mediated CSR and to gain new insights into its possible substrates, LPS and αIgM-stimulated B cells were subjected to global and phosphoproteomic analyses. We identified 103 proteins that were upregulated and 20 proteins that were downregulated in LPS stimulated B cells, while after αIgM treatment, the expression of 314 and 55 proteins was upregulated or downregulated, respectively (FC >1.5 or <-1.5, p<0.05) **(Figure 2A)**. Using the Metascape database for the analysis of datasets at the systems level[36], we found that DYRK1A is involved in the cell cycle progression and DNA damage and repair pathways **(Figure 2B)**. Since DYRK1A is a kinase[25,37], we next used phosphoproteomics analysis to screen for specific targets that could potentially explain the defect in CSR. In this analysis, a potential target site was considered as differentially phosphorylated if its phosphorylation level significantly changed in *Dyrk1a*-deficient B cells compared to WT (FC >1.5 or <-1.5, p<0.05). Protein sites were excluded if their protein level was significantly changed in the same direction as the phosphorylation level (FC >1.25 or <-1.25, p<0.1). This analysis revealed 181 hypophosphorylated sites in LPS-stimulated B cells, and 454 hypophosphorylated sites in αIgM stimulated cells **(Figure 2C)**. Examination of the biological pathways affected by the loss of protein phosphorylation showed a robust change in biological pathways involving DNA recombination and mismatch repair **(Figure 2D)**. Specifically, the mismatch repair protein MSH6, whose total protein expression was unchanged, showed reduced phosphorylation at five different sites **(Figure 2C and E)**. This finding indicates that MSH6 may be a direct target of DYRK1A.

MSH6 was previously reported to play a key role in B cell CSR[38–41]. Since *Dyrk1a*-deficient B cells showed a severe defect in this process as well, we examined whether MSH6 is a direct substrate of DYRK1A. Using recombinant DYRK1A and MSH6 proteins, the phosphotransferase activity of DYRK1A was examined in vitro. MSH6 was not phosphorylated in the absence of DYRK1A or ATP, but when both the recombinant proteins and ATP were incubated together, MSH6 acquired a phosphorylation signal. Furthermore, DYRK1A was autophosphorylated, as expected[42] **(Figure 2F)**. To examine if MSH6 phosphorylation promotes CSR, we transduced WT splenic B cells with retroviral constructs encoding WT MSH6 or an unphosphorylatable MSH6 mutant (T326A) **(Figure 2C and 2E).** Transduced B cells were stimulated with LPS and IL-4 for 3 days and examined by flow cytometry for IgG1 class-switching. Although the results of this assay were quite variable, the frequency of IgG1 class-switched *Msh6T326A* transduced B cells was significantly reduced compared to the control **(Figure 2G)**. It is important to note that endogenous WT MSH6 was also expressed in the B cells that were transduced with *Msh6T326A,* and additional DYRK1A phosphorylation sites on MSH6 might also play a role in CSR. Nonetheless, the reduction in class switching was significant, demonstrating that phosphorylation of MSH6 at the DYRK1A-targeted site is required for intact CSR.

Figure 2

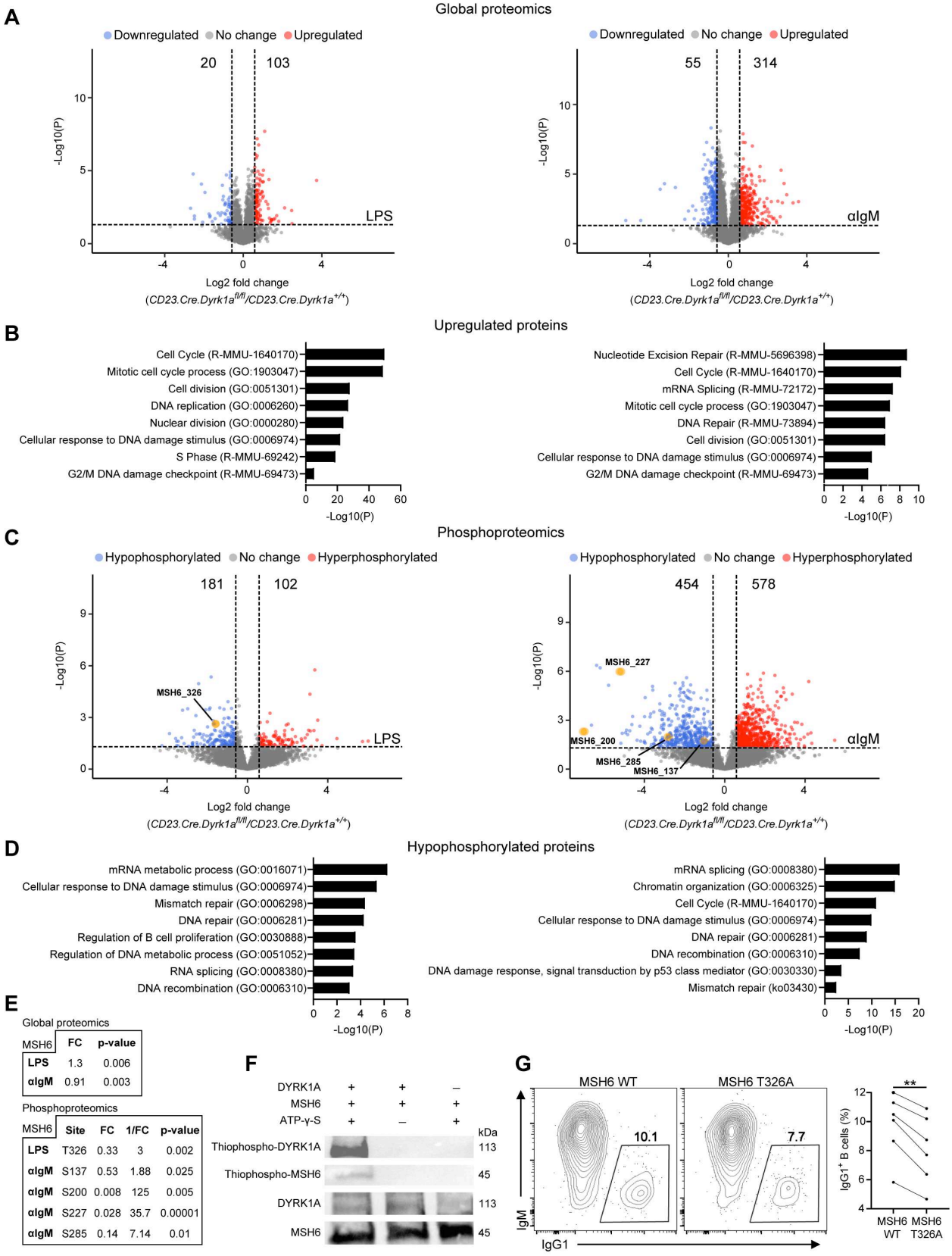

Global proteomics

MSH6	FC	p-value
LPS	1.3	0.006
αIgM	0.91	0.003

Phosphoproteomics

MSH6	Site	FC	1/FC	p-value
LPS	T326	0.33	3	0.002
αIgM	S137	0.53	1.88	0.025
αIgM	S200	0.008	125	0.005
αIgM	S227	0.028	35.7	0.00001
αIgM	S285	0.14	7.14	0.01

Figure 2. MSH6 is a direct target of DYRK1A phosphorylation. (A, B) Volcano plots depicting changes in protein expression in *Dyrk1a*-deficient B cell mice compared to littermates, which were stimulated with LPS or αIgM for 3 days (A), and biological pathways analysis performed on upregulated proteins (B). **(C, D)** Volcano plots showing changes in specific phosphorylation sites (C) and biological pathways analysis performed on hypophosphorylated sites in B cells stimulated with LPS or αIgM for 3 days (D). (n=5; three independent experiments). Colored points correspond to p value < 0.05 and log2 FC > 0.58 (red) or <-0.58 (blue). **(E)** Table listing detected MSH6 global (top) and phosphoproteomic (bottom) changes. **(F)** Representative western blot showing an in vitro direct kinase assay (two independent experiments). **(G)** Representative flow cytometry plots and frequencies of $IgG1^+$ WT B cells transduced with either MSH6 WT or MSH6 T326A retroviral constructs and stimulated in-vitro with LPS + IL-4 for 3 days (n=6; two independent experiments, paired Student's t-test). The connected dots represent data from the same mouse; ** $P \leq 0.01$.

B cell class switch recombination in vivo requires DYRK1A

To examine whether DYRK1A regulates CSR in vivo, the presence of class-switched antibodies in the serum of *CD23.Cre.Dyrk1a*$^{fl/fl}$ mice was examined by ELISA. Serum immunoglobulins derived from unmanipulated mice revealed reduced titers of class-switched antibodies in *CD23.Cre.Dyrk1a*$^{fl/fl}$ mice, including IgA, IgG1 and IgG2b, whereas IgM titers were unchanged compared with control mice **(Figure 3A)**. Nonetheless, the total number of bone marrow (BM) PCs in *Dyrk1a*-deficient mice was similar to the controls, suggesting that a defect in generation of these cells cannot explain the lack of class-switched antibodies in the mouse sera **(Figure 3B)**. Intracellular staining for Ig isotypes revealed a significant reduction in $IgG1^+$ PCs in the BM of *CD23.Cre.Dyrk1a*$^{fl/fl}$ mice **(Figure 3B)**. These results indicate that DYRK1A plays a role specifically in the generation of class-switched antibodies rather than in PC formation.

The GC reaction is the major source for class-switched antibody-secreting cells. To examine whether the reduced frequency of class-switched PCs in *CD23.Cre.Dyrk1a*$^{fl/fl}$ mice is a result of an impaired GC response, *CD23.Cre.Dyrk1a*$^{fl/fl}$ and littermate mice were immunized subcutaneously in the hind footpads with hapten (4-hydroxy-3-nitrophenyl [NP]) coupled to

keyhole limpet hemocyanin (KLH) in alum. Flow cytometric analysis 7 days later, revealed that the frequency of GC B cells was not altered in the absence of DYRK1A **(Figure 3C)**. Nonetheless, and consistent with the findings we described under homeostatic conditions, the frequency of $IgG1^+$ class-switched B cells in *Dyrk1a*-deficient GCs was significantly lower compared to the controls **(Figure 3C)**. Since CSR primarily occurs prior to the establishment of mature GCs[10], we conclude that DYRK1A plays a role in the generation of class-switched B cells at early stages of the immune response.

To understand whether DYRK1A in B cells plays a protective role during pathogen invasion, *CD23.Cre.Dyrk1a*$^{fl/fl}$ and control mice were infected with Vesicular Stomatitis Indiana Virus (VSV-Ind), which is cleared from the host through an antibody-mediated immune response[3]. After 1 week following systemic infection, significant weight loss was observed among the *CD23.Cre.Dyrk1a*$^{fl/fl}$ mice, whereas the control mice recovered by day 7 post-infection and their body weight started to increase. By day 21 post-infection, 7 out of 12 (58%) *CD23.Cre.Dyrk1a*$^{fl/fl}$ mice died, while only 1 out of 9 (11%) control mice died **(Figure 3D)**. We conclude that DYRK1A in B cells plays a key role in mounting a protective immune response against VSV-Ind.

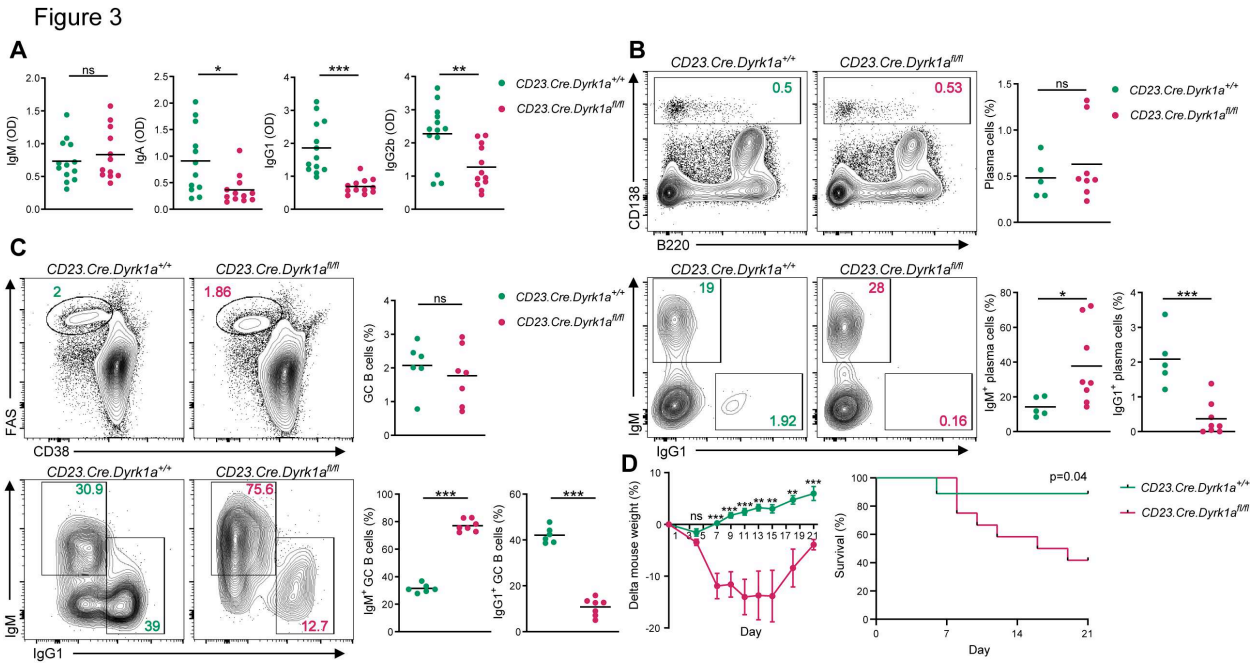

Figure 3. B cell class switch recombination in vivo requires DYRK1A. (A) Serum IgM, IgA, IgG1 and IgG2b titers as determined by ELISA (n=12-13 unmanipulated mice; two independent experiments, two-tailed student's t-test). **(B)** Representative flow cytometry plots and frequencies of total and IgG1$^+$ BM PCs in unmanipulated mice (n=5-8; three independent experiments, two-tailed student's t-test). **(C)** Representative flow cytometry plots and frequencies of total GC and isotype-specific GC B cells in popliteal LNs 7 days after NP-KLH immunization (n=6-7; two independent experiments, two-tailed Student's t-test). **(D)** Time course of changes in mouse weight and survival following i.v. VSV-Ind infection (n=9-12 mice; two independent experiments, multiple two-tailed Student's t-tests, and the Log-rank Mantel-Cox test). Each dot in the graphs represents a single mouse; * P=0.05, ** P≤0.01, ***P≤0.001, ns, not significant.

DYRK1A restricts the germinal center size

MSH6 is important for both the proper acquisition of CSR, which primarily takes place after the initial B cell activation, and for SHM, occurring during the GC reaction. To examine the role of DYRK1A in SHM, we first examined the GC response in immunized mice. To overcome the CSR defect, we crossed *Dyrk1a*$^{fl/fl}$ mice with *Aicda*$^{Cre/+}$ and *Rosa26*$^{flox\text{-}stop\text{-}flox\text{-}tdTomato}$ mice. AID (encoded by *Aicda*) is upregulated during initial B cell activation, after T cell-dependent antigen encounter, and prior to GC seeding[10,43–45]. Since CSR occurs after AID expression but before GC formation, this model allowed us to bypass the early defects and examine class-switched B cells in the GC response. In contrast to the results obtained using the *CD23.Cre* model, under homeostasis, increased IgG1 titers were detected in *AID.Cre.Dyrk1a*$^{fl/fl}$ mice, while IgA and IgG2b titers did not change significantly **(Figure 4A)**. While the overall frequency of PCs in the BM of *AID.Cre.Dyrk1a*$^{fl/fl}$ mice was not altered, a 2-fold increase in IgG1^{+} PCs was detected in these mice compared to control animals **(Figure 4B)**. Thus, we conclude that DYRK1A plays a critical role in CSR in the early response, while it does not play a role in later events, such as in maintenance of class-switched PCs.

Since most of the class-switched PCs originate from the GC, we examined whether changes occur in this compartment in immunized *AID.Cre.Dyrk1a*$^{fl/fl}$ mice. Flow cytometric analysis 7 days after immunization with NP-KLH, revealed that the frequency of GC B cells and PCs in the draining LNs of *AID.Cre.Dyrk1a*$^{fl/fl}$ mice was significantly increased compared to littermate controls **(Figure 4C)**. Similarly, since CSR occurs prior to GC formation but after AID expression, no defect in the frequency of IgG1^{+} GC B cells was observed **(Figure 4C)**. The increased frequency of GC B cells detected by flow cytometry could indicate either larger GC compartments or an increased number of individual GCs. To resolve this issue, we used intravital two-photon laser

microscopy (TPLM) to image the popliteal LNs of immunized control and *AID.Cre.Dyrk1a*$^{fl/fl}$.*Rosa26*$^{flox\text{-}stop\text{-}flox\text{-}tdTomato}$ mice. This approach revealed that the size of each individual GC was significantly larger in the *AID.Cre.Dyrk1a*$^{fl/fl}$ compared to control mice **(Figure 4D)**. To determine whether the elevated size of GCs that we observed after immunization with a model antigen is reproducible in an infection model, we infected mice with VSV-Ind. Similar to the vaccination model, 7 days after VSV-Ind injection to the footpad of *AID.Cre.Dyrk1a*$^{fl/fl}$, the frequency of GC B cell in the draining popliteal LNs was higher compared to control mice, though the frequency of PCs and class-switched B cells did not change in this setting **(Figure 4E)**. Collectively, we conclude that after initial B cell activation and CSR, DYRK1A restrains GC size during a response to vaccination or virus infection.

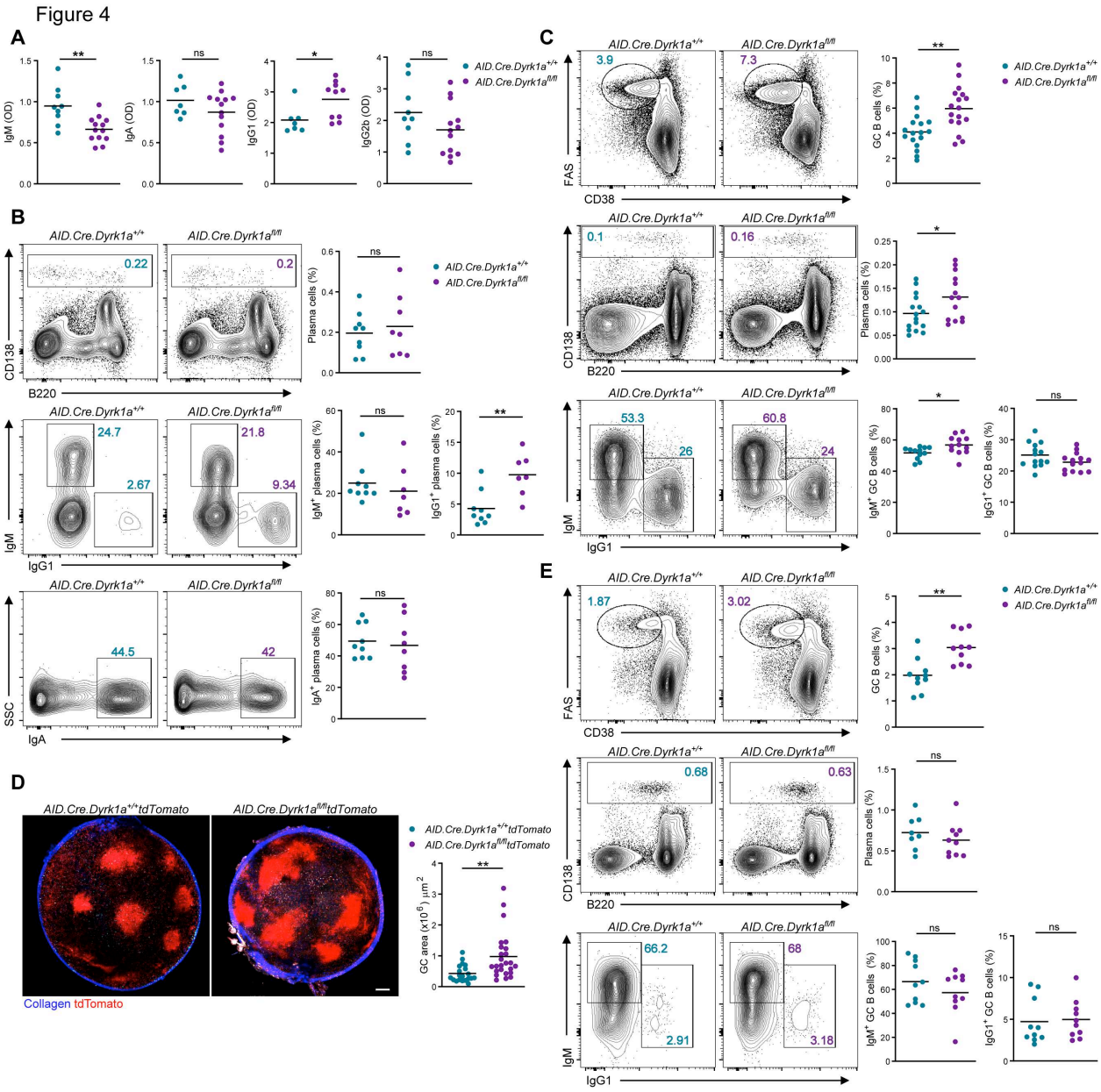

Figure 4. DYRK1A restricts the magnitude of the B cell immune response. (A) Serum IgM, IgA, IgG1 and IgG2b titers as measured ELISA (n=7-13 unmanipulated mice; two independent experiments, two-tailed Student's t-test). **(B)** Representative flow cytometry plots and frequencies of total and class-switched PCs in the BM of unmanipulated mice (n=7-9; two independent experiments, two-tailed Student's t-test). **(C)** Representative flow cytometry plots and frequencies of total GC, PC, and isotype-specific GC B cells in popliteal LNs 7 days after NP-KLH immunization (n=12-17; three independent experiments, two-tailed Student's t-test). **(D)** Representative TPLM images of popliteal LN-derived from *AID.Cre.Dyrk1a*$^{fl/fl}$*.Rosa26*$^{flox\text{-}stop\text{-}flox\text{-}tdTomato}$ mice and quantification of GC area 7 days after NP-KLH immunization. Each dot in the graph represents a single GC (n=3-5; three independent experiments, two-tailed Student's t-test);

scale bar 200μm. **(E)** Representative flow cytometry plots and frequency quantification of total GC, PC, and isotype-specific GC B cells in popliteal LNs 7 days after VSV-Ind infection (n=8-10; two independent experiments, two-tailed Student's t-test). Each dot in the graphs represents a single mouse; * P=0.05, ** P≤0.01, ***P≤0.001, ns, not significant.

DYRK1A is required for antigen-specific clonal expansion

Msh6-deficient mice have altered SHM patterns in their B cell immunoglobulin genes[39]. To examine if DYRK1A plays a role in clonal expansion and insertion of SHM in the GC reaction, we sorted single $IgG1^+$ GC B cells from the LNs of NP-KLH immunized mice, followed by *Ighg1* amplification and sequencing[46]. This analysis revealed that the magnitude of clonal expansion and diversity in the control versus *Dyrk1a*-deficient mice was similar to wild type both 7 and 21 days post-immunization **(Figure 5A)**, as was the specific V-region usage **(Figure 5B).** *Dyrk1a*-deficient B cells acquired SHM in their variable region to a lesser extent compared to the control mice, but although this difference was statistically significant, it was relatively small **(Figure 5C).** Furthermore, lineage tree reconstruction of representative expanded clones revealed that *Dyrk1a*-deficient B cells diversify and accumulate SHMs in the GC, suggesting that the GC reaction supports antibody-affinity maturation **(Figure 5D)**. To further understand whether DYRK1A has a role in affinity maturation and selective antigen-specific clonal expansion, we specifically inspected *IGHV1-72*, which is the typical clone that responds to NP in C57B/6 mice[47]. For this purpose, we used shared clone analysis which demonstrates clonal expansion of specific V-J *Ighg1* sequences. Both control and *AID.Cre.Dyrk1a*$^{fl/fl}$ hosted individual GC B cells bearing *IGHV1-72* 7 days after the immunization. In control mice, the presence of these clones increased after an additional 14 days, demonstrating clone-specific expansion in these GCs. In contrast, in *AID.Cre.Dyrk1a*$^{fl/fl}$ mice, *IGHV1-72* B cell clones were not clonally expanded, and a clone that carries a different BCR, *IGHV1-22*, dominated the GC response in one mouse, whereas in the

second mouse, no clonal expansion of *IGHV1-72* or of other shared clones was observed **(Figure 5E)**. To examine if the defect in clonal expansion of antigen-specific B cells that carry *IGHV1-72* is a result of failure in the selection of B cells that acquired affinity-enhancing SHMs, we quantified the frequency of two mutations that are associated with increased immunoglobulin affinity, W33L and K59R. The presence of these mutations was comparable in littermates and *AID.Cre.Dyrk1a*$^{fl/fl}$ mice, suggesting that B cell selection is not impaired in *Dyrk1a*-deficient GC B cells **(Figure 5F)**. We conclude that DYRK1A is required for proper clonal expansion of antigen-specific GC B cells that carry high-affinity BCRs.

DYRK1A is not required for nucleotide base substitutions during somatic hypermutation

We demonstrated that DYRK1A regulates CSR through phosphorylation of MSH6 early in the response, and this kinase also controls the magnitude of the GC reaction at later time points. In addition to its role in CSR, MSH6 was suggested to modulate the pattern of specific SHM in GCs[39,48]. To examine whether DYRK1A controls B cell functions in the GC through MSH6 activity, we further investigated the mutational landscape of *Ighg1* in *AID.Cre.Dyrk1a*$^{fl/fl}$ mice. For this purpose, we re-examined the *Ighg1* sequences to identify specific nucleotide substitutions that might be affected by the lack of MSH6 functions. Furthermore, since this analysis was previously done using immunoglobulin sequences derived from PPs, we also sequenced *Ighg1* from PP GCs of 1-year-old control and *AID.Cre.Dyrk1a*$^{fl/fl}$ mice. Analysis of specific changes in the mutational patterns showed no differences in nucleotide substitutions in *Dyrk1a*-deficient B cells compared to the control mice in either draining LNs or PPs **(Figure 5G)**. These results suggest that SHMs are not regulated through DYRK1A and MSH6 phosphorylation in the GC.

Figure 5

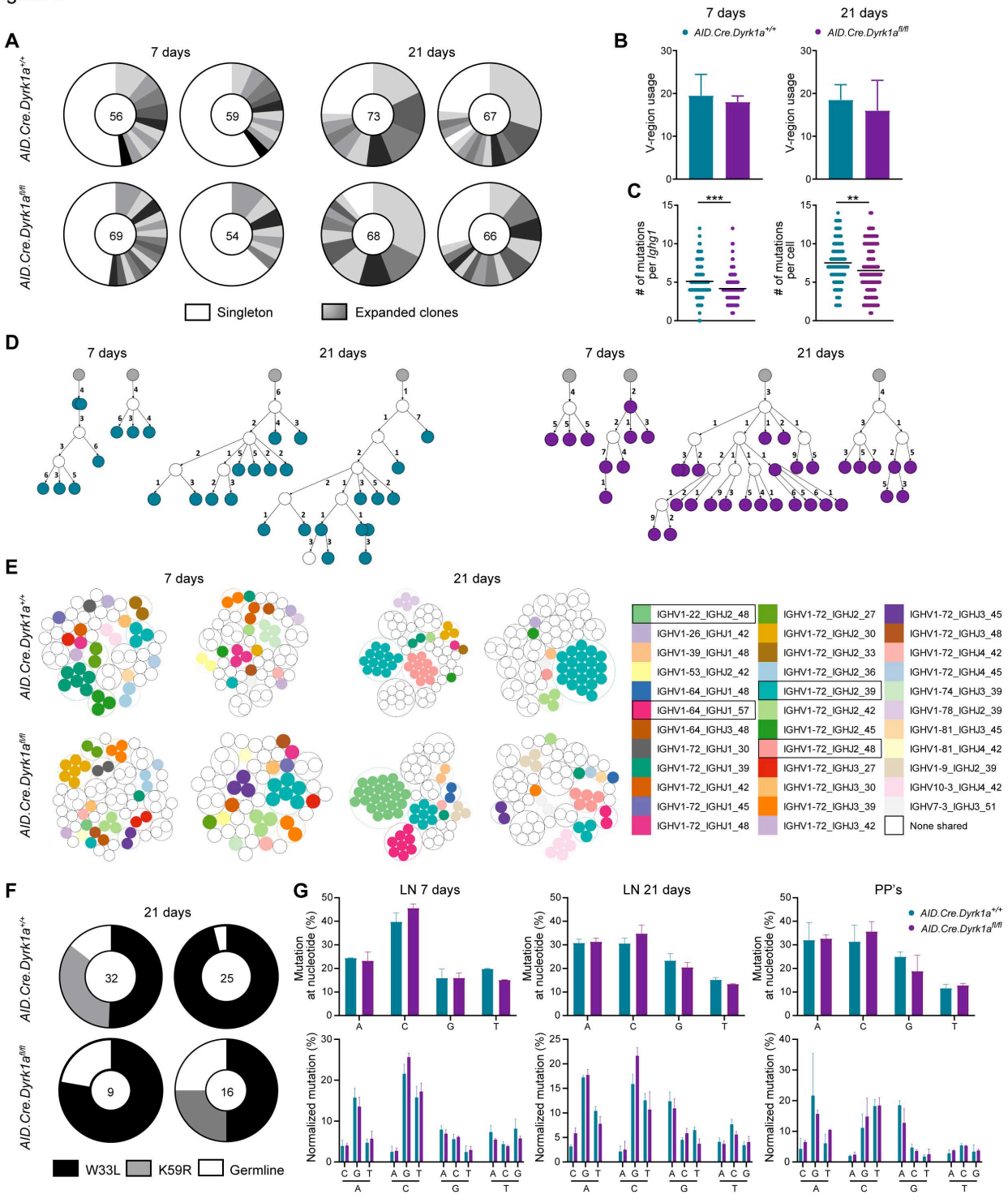
A
7 days
21 days
AID.Cre.Dyrk1a+/+
AID.Cre.Dyrk1afl/fl
56
59
73
67
69
54
68
66
Singleton
Expanded clones
B
7 days
21 days
AID.Cre.Dyrk1a+/+
AID.Cre.Dyrk1afl/fl
V-region usage
C
***
**
# of mutations per Ighg1
# of mutations per cell
D
7 days
21 days
7 days
21 days
E
7 days
21 days
AID.Cre.Dyrk1a+/+
AID.Cre.Dyrk1afl/fl
IGHV1-22_IGHJ2_48
IGHV1-26_IGHJ1_42
IGHV1-39_IGHJ1_48
IGHV1-53_IGHJ2_42
IGHV1-64_IGHJ1_48
IGHV1-64_IGHJ1_57
IGHV1-64_IGHJ3_48
IGHV1-72_IGHJ1_30
IGHV1-72_IGHJ1_39
IGHV1-72_IGHJ1_42
IGHV1-72_IGHJ1_45
IGHV1-72_IGHJ1_48
IGHV1-72_IGHJ2_27
IGHV1-72_IGHJ2_30
IGHV1-72_IGHJ2_33
IGHV1-72_IGHJ2_36
IGHV1-72_IGHJ2_39
IGHV1-72_IGHJ2_42
IGHV1-72_IGHJ2_45
IGHV1-72_IGHJ2_48
IGHV1-72_IGHJ3_27
IGHV1-72_IGHJ3_30
IGHV1-72_IGHJ3_39
IGHV1-72_IGHJ3_42
IGHV1-72_IGHJ3_45
IGHV1-72_IGHJ3_48
IGHV1-72_IGHJ4_42
IGHV1-72_IGHJ4_45
IGHV1-74_IGHJ3_39
IGHV1-78_IGHJ2_39
IGHV1-81_IGHJ3_45
IGHV1-81_IGHJ4_42
IGHV1-9_IGHJ2_39
IGHV10-3_IGHJ4_42
IGHV7-3_IGHJ3_51
None shared
F
21 days
AID.Cre.Dyrk1a+/+
AID.Cre.Dyrk1afl/fl
32
25
9
16
W33L
K59R
Germline
G
LN 7 days
LN 21 days
PP's
AID.Cre.Dyrk1a+/+
AID.Cre.Dyrk1afl/fl
Mutation at nucleotide (%)
Normalized mutation (%)

Figure 5. Antigen-specific clonal expansion but not SHM depends on DYRK1A functions. **(A)** Pie charts showing the clonal distribution of *Ighg1* sequences in GC B cells derived from one LN of a single mouse, 7 or 21 days after NP-KLH immunization. Each slice represents a unique clone. The total number of analyzed sequences is indicated in the center of each chart (n=2; two independent experiments). **(B)** The number of different V-regions detected in *Ighg1* sequences as in A. Bars and error bars represent the mean with SD. **(C)** The number of SHMs per analyzed sequence as in A. **(D)** Phylogenic trees of representative individual clones. Gray circles represent the hypothetical germline configuration. White circles represent hypothetical ancestors. Numbers appearing next to the arrows represent the number of distinct mutations accumulated between clonal members. **(E)** Shared clone analysis of the sequences as in A. Each color represents an individual shared clone. White represents clones detected in one LN and not in the others (non-shared). **(F)** The frequency of single cells bearing the NP-specific high-affinity mutations in the *Ighv1-72* heavy chain gene, 21 days after immunization. The total numbers of analyzed *Ighv1-72* sequences are indicated in the center of each chart. **(G)** Analysis of the mutational landscape showing total mutations at each base position and individual nucleotide substitutions in *Ighg1* sequences from GC B cells derived from one LN of a single mouse 7 or 21 days after NP-KLH immunization, or a single PP. Bars and error bars represent the mean with SD (n=2; two independent experiments); ** $P \leq 0.01$, *** $P \leq 0.001$.

DYRK1A is a negative regulator of cell cycle progression in GC B cells

The role of DYRK1A in the regulation of cell cycle events was shown previously in tumor, neuronal, fibroblastic, and pre-B cells [25,27–29,49]. Thus, we examined the possibility that DYRK1A controls GC size by modulating the cell cycle progression of B cells within the GC. The GC is composed of two zones, the dark zone (DZ), where B cells undergo clonal expansion and diversify their immunoglobulins by SHM, and the light zone (LZ), where B cells are subjected to selection based on their BCR affinity[9,50]. We found that GCs in the draining popliteal LNs of immunized *AID.Cre.Dyrk1a*$^{fl/fl}$ mice exhibit smaller DZ compartments compared to their control counterparts **(Figure 6A)**. To examine whether DYRK1A controls gene expression profiles and biological pathways that may explain the observed changes in GC size, we sorted LZ and DZ B cells and subjected them to RNA-seq analysis. We found in the DZ 747 genes that were upregulated, and 516 genes that were downregulated when compared to control cells (log2 FC $\geq \pm 0.58$, adjusted p

< 0.05). A change in expression of only 28 genes was detected in the LZ, suggesting that DYRK1A plays a minor if any role in this GC compartment. **(Figure 6B)**.

Utilizing the Metascape tool to identify the biological processes associated solely with the upregulated gene profile of DZ B cells, we found that in the absence of DYRK1A, cell cycle, DNA replication, nuclear division and DNA repair events are massively altered **(Figure 6C)**, providing an explanation for the enlarged GC size we observed **(Figure 4)**. To identify signaling pathways that were modified in *Dyrk1a*-deficient DZ B cells, we analyzed the gene signatures by gene set enrichment analysis (GSEA). This analysis revealed significant changes in genes related to the G2M and E2F pathways, known entry checkpoints to DNA synthesis and mitosis phases[51,52] **(Figure 6D)**. To determine whether the detected cell division transcriptomic changes indeed affect the B cell cycle, we injected immunized mice with the nucleoside analog EdU, which is incorporated into newly formed DNA in dividing cells. Flow cytometric analysis of GC B cells revealed that the fraction of both total EdU incorporating cells, and specific cells in the S-phase, was significantly higher in *Dyrk1a*-deficient B cells **(Figures 6E and 6F)**. We therefore conclude that DYRK1A negatively regulates expression of genes involved in the cell cycle and modulates multiple proliferation factors primarily in the DZ, the major site at which B cells divide and expand in the GC.

Figure 6

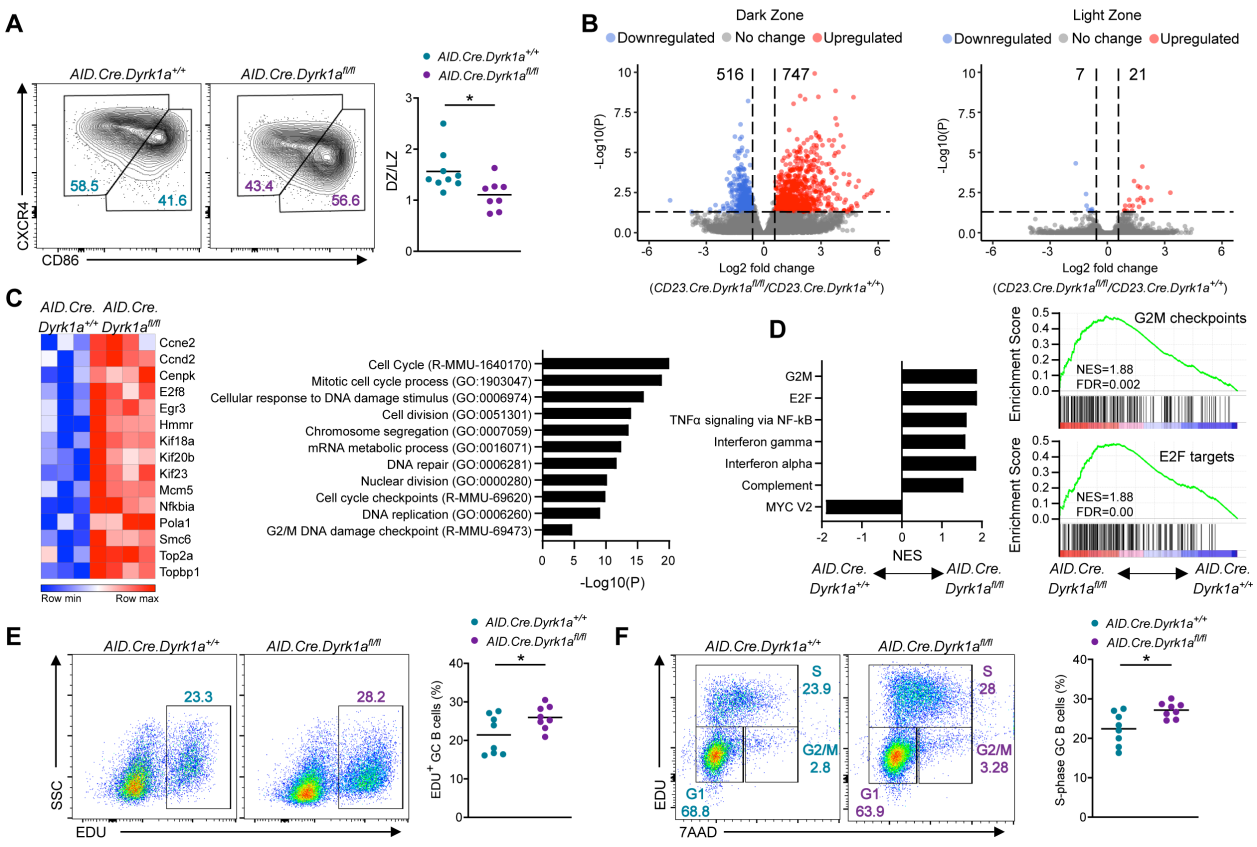

Figure 6. DYRK1A is a negative regulator of cell cycle progression in GC B cells. (A) Representative flow cytometry plots and ratio of DZ to LZ GC B cells in popliteal LNs 7 days after NP-KLH immunization (n=8-9; four independent experiments, two-tailed Student's t-test). **(B)** Volcano plots showing differential gene expression in the LZ and DZ of GC B cells derived from mice, as in A (n=3-4; two independent experiments). Colored points correspond to adjusted p value < 0.05 and log2 FC > 0.58 (red) or <-0.58 (blue). **(C)** Heatmap of differentially expressed genes and biological pathway analysis of upregulated genes of DZ B cells, as in A. **(D)** GSEA analysis of upregulated DZ B cell gene expression profiles from mice as in A. NES, normalized enrichment score; FDR, false discovery rate. **(E,F)** Analysis of the different cell cycle stages in GC B cells by EdU incorporation and 7AAD DNA staining 7 days after NP-KLH immunization (n=8; three independent experiments, two-tailed Student's t-test). SSC, side scatter. Each dot in the graph represents a single mouse; * P=0.05, ** P≤0.01, ***P≤0.001, ns, not significant.

Discussion

CSR is critical for the generation of antibodies with the capacity to clear infected or malignant cells, by triggering immune cell effector function[5]. Here, we describe a previously unknown molecular mechanism that controls CSR recombination at the post-translational level through the functions of DYRK1A. Whereas this kinase is a master regulator of cell proliferation through targeting many cell-cycle-related proteins for degradation, we demonstrate an additional novel DYRK1A-mediated mechanism that controls CSR through MSH6 phosphorylation.

Single base nucleotide mismatches are recognized by the MutSα complex, which is composed of mismatch repair (MMR) proteins including MSH2, and either the MSH3 or MSH6 subunits[53–55]. The recruitment of this complex to the switch region leads to the excision of the mutated sites followed by DNA resynthesis by an error-prone polymerase[56,57]. Generation of mismatched nucleotides through AID enzymatic activity followed by DNA repair mechanisms is essential for CSR[40]. *Msh2*- *Msh6*- but not *Msh3*-deficient B cells are defective in this process, and indeed, MSH3 was not detected as a target for DYRK1A in our phosphoproteomics analysis, indicating that DYRK1A is not involved the regulating MSH3 functions[39,58–63]. In addition to DYRK1A, regulation of MSH6 functions by phosphorylation through the activity of PKC and casein kinase activity was previously demonstrated in other cell types[55]. However, the cells in that study did not express AID, which is unique to B cells, nor other components that support CSR specfically[11]. DYRK1A was previously linked to DNA-damage responses through phosphorylation of SIRT1 and deacylation of P53, and this mechanism is required for cell survival[64]. In contrast, we show that DYRK1A deficiency enhances cell proliferation when cells are subjected to DNA damage by AID, suggesting that P53-mediated cell survival mechanisms do not play a role in GC B cells. The MutSα complex induces the insertion of additional SHMs into the immunoglobulin locus after the

generation of nucleotide mismatch by AID activity[39,48]; however, DYRK1A-mediated phosphorylation did not play a major role in this process, suggesting that either MSH6 phosphorylation is required only for effective CSR, or that a different overlapping molecular mechanism compensates for MSH6 functions in GC B cells[48].

In contrast to CSR, the role of DYRK1A in the attenuation of cell cycle progression has been extensively described[24], but its role in B cell immune responses was not examined. A previous study demonstrated that DYRK1A plays a role in B cell development through phosphorylation of Cyclin D3, and most likely plays a similar role during mature B cell proliferation and within the GC reaction[28]. DYRK1A also phosphorylates Myc, a target that is involved in B cell selection for clonal expansion by T cells in the GC[32,33]. In line with the functions of DYRK1A in cell cycle attenuation, deletion of *Dyrk1a* after AID expression specifically affected the DZ genetic program and enhanced B cell proliferation. Nonetheless, the DZ in *AID.Cre.Dyrk1a*$^{fl/fl}$ mice was smaller, suggesting that the increase is a result of enhanced proliferation in the LZ. Lack of proper cell cycle control is expected to lead to an aberrant clonal expansion, and indeed, antigen-specific *Dyrk1a*-deficient B cell clones that carry an affinity-enhancing mutation in their immunoglobulin genes were unable to expand in the GC at the expense of other clones. We propose that enhancing *Myc* expression and proliferation of all the cells in the GC will raise the bar for the selection of specific clones for expansion. The increase in cell-cycle progression and the defect in clonal expansion of antigen-specific B cells is most likely due to a lack of proper degradation of multiple cell-cycle regulators, including Myc and Cyclins [28–33]. An additional possibility explaining the increase in GC size is enhanced infiltration of newly activated B cells into the GC[65,66] however, we did not detect a strong reduction in SHM accumulation in *Dyrk1a*-deficient B cells, suggesting that this is not the major explanation for the inability of the antigen-specific clones to dominate

the GC reaction. Thus, we conclude that in the GC, DYRK1A is a master regulator of cell cycle progression, which supports the proper expansion of selected clones and maintains proper GC size. Although we directly show that MSH6 is a target for DYRK1A, additional targets in this pathway cannot be completely excluded. Whereas CSR did not take place in *Dyrk1a*-deficient B cells in vitro, a small IgG1+ population was detected in vivo. It is most likely that either other MMR proteins compemnstae for the loss of MSH6 in vitro but not in vivo. Furthermore, we have observed a significant but modest reduction in CSR upon removal of one phsphrylation site from MSH6, suggesting that other target sites most play a role as well.

Collectively, this study demonstrates two major roles for DYRK1A in B cell immune responses, which include control of CSR through MSH6 phosphorylation, and regulation of cell cycle in GC B cells through multiple cell-cycle factors. Several inhibitors for DYRK1A were developed for the treatment of various types of cancer[24,67] however, our results suggest that these could enhance the proliferation of GC-originated malignancies. Nonetheless, suppression of DYRK1A by these inhibitors might be useful for attenuation of CSR in autoimmune diseases and allergies.

Acknowledgments

Z.S. is supported by the European Research Council (ERC) grant No. 101001613, by the Morris Kahn Institute for Human Immunology, Human Frontiers of Science Program (CDA-00023/2016), Azrieli Foundation, Israel Science Foundation (1090/18). This study was also supported by Ben B. and Joyce E. Eisenberg Foundation, Wolfson Family Charitable Trust & Wolfson Foundation, Elie Hirschfeld and Dr. Sarah Schlesinger and Miel de Botton. Z.S. is a member of the European Molecular Biology Organization (EMBO) Young Investigator Program.

E.H. received support from the ASH Medical Student Physician-Scientist Award.

Materials and Methods

Mice

Dyrk1a$^{flox/flox}$, Aicda$^{Cre/+}$ and Rosa26$^{flox\text{-}stop\text{-}flox\text{-}tdTomato}$ mice were purchased from the Jackson Laboratory. CD23^{cre} mice were generated and provided by M. Busslinger (Research Institute of Molecular Pathology, Vienna, Austria). Mice were used at the age of 6–12 weeks. All experiments on mice were approved by the Weizmann Institute Animal Care and Use Committee.

Immunizations and infections

Mice were injected with 25 µl PBS containing 10 µg NP-KLH (BioSearch Technologies) in alum into each hind footpad. For Vesicular Stomatitis Indiana Virus (VSV-Ind) infections, mice were either injected with 10^6 PFU i.v. or with 10^5 PFU into each hind footpad.

Flow cytometry

Popliteal LNs were removed, washed in cold PBS, and forced through a 70 µm mesh into PBS containing 2% FCS and 1 mM EDTA to create single-cell suspensions. Cells were subsequently incubated with fluorescently labeled antibodies (Table S1) for 30 min on ice. Intracellular antibody staining was performed after fixation and permeabilization with Fixation/Permeabilization Solution Kit (BD Biosciences). GC cells were gated as live/single, B220^{+} CD38^{Lo} FAS^{Hi}. DZ and LZ cells were gated as CXCR4^{hi} CD86^{lo} and CXCR4^{lo} CD86^{hi}. Stained cell suspensions were analyzed using a CytoFlex flow cytometer (Beckman Coulter). For RNA-seq, cells were sorted for lack of marker expression (dump^{-}: CD4^{-}, CD8^{-}, GR-1^{-}, and F4/80^{-}) in addition to expression of GC, LZ and DZ markers, and 30,000 cells were sorted directly into 100 µl Dynabeads mRNA direct kit lysis/binding buffer (Life Technologies) using a FACS ARIA cell sorter (BD), and immediately frozen on dry ice.

ELISA

Serum was collected from un-immunized mice, and IgM, IgA, IgG1 and IgG2b titers were determined by ELISA using goat anti-mouse IgM, IgA, IgG1 and IgG2B–horseradish peroxidase (Abcam), respectively.

In Vitro CSR and proliferation assays

Spleens were removed, washed in cold PBS, and forced through a 70 μm mesh into PBS containing 2% FCS and 1 mM EDTA to create single-cell suspensions. For the proliferation assay, splenic cells were stained with CellTrace Violet (Invitrogen) according to the manufacturer's instructions. Cells were seeded at 1×10^6/ml in a 24-well plate and incubated at 37°C in B cell medium (RPMI-1640 medium supplemented with 10% FBS, 100 μg/ml penicillin/streptomycin, 50 μg/ml gentamycin, 2 mM glutamine and pyruvate, nonessential amino acids, and 50 μM β-mercaptoethanol). For CSR assay, cells were stimulated with 10 μg/ml LPS and 20ng/ml murine IL-4 for 3 days. For the proliferation assay, cells were stimulated with 10 μg/ml LPS or αIgM for 3 days. CellTrace Violet dilution was assessed by flow cytometry.

EdU proliferation assay

NP-KLH immunized mice were injected i.v. with 2 mg of the nucleoside analogue 5-ethynyl-2′-deoxyuridine EdU (Molecular Probes) in PBS. After 2.5 h, popliteal LNs were stained for the surface antigens B220, CD38, FAS and CD138, followed by EdU detection using the Click-iT EdU Alexa Fluor 647 Flow Cytometry Assay Kit (Molecular Probes) according to the manufacturer's instructions. 7AAD (BD Biosciences) was added at 1:50 dilution 5 min before analysis by flow cytometry.

TPLM image acquisition

A Zeiss LSM 880 upright microscope fitted with a Coherent Chameleon Vision laser was used for imaging experiments. Whole lymph nodes were dissected, and images were acquired with a femtosecond-pulsed two-photon laser tuned to 940 nm. The microscope was fitted with a filter cube containing 565 LPXR to split the emission to a PMT detector (with a 579–631-nm filter for germinal center tdTomato fluorescence). Tile images were acquired as 100–200μm Z stacks with 5μm intervals between each Z plane. The zoom was set to 1.5, and images were acquired at 512 × 512 x-y resolution. Quantification of the GC area was done using the surface module of Imaris software (Bitplane).

In vitro kinase assay

100ng of recombinant DYRK1A (ThermoScientific), 5mg of recombinant MSH6 (Origene), 200μM ATP-g-S (Abcam), and kinase buffer (40mM Tris, pH 7.5, 10mM $MgCl_2$, 50mM NaCl) were combined in a 30 μL reaction. Samples were then placed in a Thermocycler at 30°C and rotated at 1000rpm for 30 minutes. To alkylate the proteins, 2.5mM of p-Nitrobenzyl mesylate (PNBM; Abcam) was added and the reaction was allowed to proceed for 2 hours at room temperature. Afterwards, loading dye was added, and samples were heated for 5 minutes at 95°C and immediately run for western blotting. Samples were loaded into Biorad Mini-PROTEAN TGX precast gels and run on the BioRad PowerPac HC system. Blots were transferred using the Bio-Rad Trans-Blot Turbo Transfer System. Samples were then blocked in 5% milk in TBST for 1 hour at room temperature. Primary antibodies (1:1000) were incubated in 5% milk overnight at 4°C. Samples were washed 3 times in 5-minute increments with TBST at room temperature before incubation with secondary antibody (1:10,000). Blots were visualized using the Biorad Chemidoc system and analyzed using Image Lab 6.1. All antibodies used are listed in Table S1.

Retrovirus production and transduction.

Platinum-E cells (Cell Biolabs) were grown to 70–80% confluence in 10-cm dishes and transfected with 10 μg of pMSCV:IRES:EGFP MSH6 WT or MSH6 T326A plasmid (VectorBuilder) diluted in 1 ml Opti-MEM and 40 μl Turbofect (ThermoFisher). Retrovirus-containing supernatants were collected 48-72 h after transfection. Fresh virus was concentrated by adding 1/3 viral volume of Retro-X concentrator (Takara Bio), overnight incubation at 4°C, and centrifugation at 1500g for 45 minutes at 4°C. Splenic B cells from WT mice were column purified using the CD43 (Ly-48) microbead kit (Milteny Biotec) and 2×10^6 cells were stimulated overnight at a final concentration of 2.5 μg/ml (1:400 dilution) αCD180 (Biolegend, clone RP/14) diluted in B cell media. The next day, stimulated B cells were washed and transduced by adding concentrated virus resuspended in B cell media and Polybrene (Sigma) at a final concentration of 10 μg/ml. Spinoculation was performed at 2500 rpm for 90 minutes at 32°C. Cells were then incubated for 3 hours at 37°C, followed by a second spinoculation. Transduced cells were then incubated at 37°C for 48h, washed 4 times, and stimulated with 20 μg/ml LPS and 40 ng/ml murine IL-4 for 3 days.

Western blot analysis

Naive splenic B cells were isolated using anti-CD43 magnetic beads (Miltenyi Biotec). Purified B cells were kept unstimulated, or stimulated with 10 μg/m LPS for 3 days. The cells were then lysed in radioimmunoprecipitation assay buffer (10 mM Tris-HCl, 1mM EDTA, 0.5mM EGTA, 1% Triton-100 140 mM NaCl, 0.1% deoxycholate, 0.1% SDS). Lysates were centrifuged for 15 min at 4°C. Cleared lysates were boiled with sample buffer for 5 min, separated by SDS-PAGE (Bio-Rad), and transferred to nitrocellulose membranes. Blots were blocked with 5% skim milk in TBST and 0.05% Tween-20 for 1 h at room temperature, and incubated with primary antibody diluted 1:1000 overnight at 4°C. Horseradish peroxidase–conjugated donkey anti-rabbit secondary antibody diluted 1:5000 and ECL Reagent (Biological Industries) were used for detection. All antibodies are listed in Table S1.

Single-cell IgH sequencing

Popliteal LNs from immunized mice or Peyer's patches from aged mice (1 year old) were harvested and processed for flow cytometry analysis. Cell suspensions were stained for dump$^-$ (CD4, CD8, GR-1, F4/80) and B220, CD38, FAS and IgG1 (BioLegend) expression. Cell sorting was performed using a FACS Aria cell sorter (BD Bioscience). GC cells were gated as live/single, B220$^+$ CD38^{Lo} FAS^{Hi}. GC-derived IgG1 B cells were sorted into 96 well plates containing lysis buffer (PBS with 3 U/µl RNAsin, 10 mM dithiothreitol). cDNA was purified using random primers (NEB) as previously described[68]. Nested PCR was used to amplify a segment of Igγ1 heavy chains using the outer constant primers (5′-GGAAGGTGTGCACACCGCTGGAC-3′) together with a mix of primers for the variable regions[68], followed by a second reaction with the inner constant (5′-GCTCAGGGAAATAGCCCTTGAC-3′) and variable primers (5′- GGGAATTCGAGGTGCAGCTGCAGGAGTCTGG-3′). Amplification conditions were as follows: 98°C for 30 s, 30 cycles of [98°C for 30 s, 50°C for 30 s, and 72°C for 30 s] (reaction I), or 40 cycles of [98°C for 30 s, 55°C for 30 s, and 72°C for 30 s] (reaction II), followed by 72°C for 2 min. PCR products were sequenced by Sanger sequencing. Sequences were aligned to the IMGT mouse heavy chain gene database (downloaded Dec. 2019) [69] using NCBI IgBlast (version 1.17.0)[70], and processed using Change-O v 1.2.0[71]. Downstream analysis of clustering, mutational load, and diversity was performed using Change-O v1.2.0[71], Alakazam v1.2.0[71], SHazaM v1.1.0[71], and custom scripts within the R v4.1.0 statistical computing environment. Clonal inference of the V(D)J sequences was based on identical IGHV and IGHJ gene annotations, and the length of the junction region. Based on these inferences, full germline sequences and phylogenetic trees were constructed for each clone. The analysis of the mutations and diversity was deduced from the phylogenetic tree of each clone using a custom R v4.1.0 script.

RNA sequencing

Popliteal LNs from mice immunized 7 days previously were harvested and sorted for GC DZ and LZ B cells based on the following staining: dump− (CD4, CD8, GR-1, F4/80) and B220+ CD38− FAS+, followed by CXCR4+ CD86− or CXCR4− CD86+, representing DZ or LZ cells, respectively. For gene expression analysis, 3×10^4 cells from each population were sorted into 100 µl lysis/binding buffer and mRNA was captured using the Dynabead mRNA direct kit according to the manufacturer's instructions (Life Technologies). A bulk adaptation of the massively parallel single-cell RNA sequencing protocol (MARS-seq) was used as previously described[72,73] to generate RNA-seq libraries for transcriptomic analysis. Alignment and differential expression analysis was performed using the UTAP pipeline[74]. Reads were trimmed using Cutadapt and mapped to the Mus musculus genome (UCSC mm10) using STAR[75] v2.4.2a with default parameters. The pipeline quantifies the genes annotated in RefSeq (extended by 1,000 bases toward the 5′ edge and 100 bases in the 3′ direction). Htseq-count [76] (union mode) was used for counting sequenced reads. Expression analysis was based on genes with a minimum of five UMI-corrected reads in at least one sample. Normalization of the counts and differential expression analysis was performed using DESeq2[77]. Raw P values were adjusted for multiple testing using the procedure of Benjamini and Hochberg. Differentially expressed genes were visualized using the EnhancedVolcano R package. The threshold for significant differential expression was $\log_2 FC > 0.58$ or <-0.58, $p<0.05$. GSEA was performed using GSEA 4.1 with the GSEA preranked tool[78]. Gene names were converted to human gene symbols, and run with default parameters. The Molecular Signature Database hallmark gene sets were used to perform pathway enrichment analysis using a hypergeometric distribution, and limiting the output to the top 100 gene sets. The Metascape tool was used to define unique pathways that were significantly modified using the threshold mentioned above[36].

Sample preparation for proteomics analysis

Splenic B cells were column purified using the CD43 (Ly-48) microbead kit (Milteny Biotec), and 8×10^6 cells were stimulated with 10µg/ml LPS or 10µg/ml αIgM for 3 days. Cells were washed twice with cold PBS, and resuspended in 80 µl lysis buffer (50 mM Tris pH 7.6, 5% SDS and 1% phosphatase inhibitors cocktails 2 and 3 (Sigma)). Lysates were incubated at 95°C for 5 minutes, and sonicated for six cycles of 30 s (Bioruptor Pico, Diagenode, USA). Protein concentration was measured using the BCA assay (Thermo Scientific, USA) and a total of 120 µg protein was reduced with 5 mM dithiothreitol (Sigma) and alkylated with 10 mM iodoacetamide (Sigma) in the dark. Each sample was loaded onto S-Trap minicolumns (Protifi, USA) according to the manufacturer's instructions. In brief, after loading, samples were washed with 90:10% methanol/50 mM ammonium bicarbonate. Samples were then digested with trypsin (1:50 trypsin/protein) for 1.5 h at 47°C. The digested peptides were eluted using 50 mM ammonium bicarbonate; trypsin was added to this fraction and incubated overnight at 37°C. Two more elutions were performed using 0.2% formic acid and 0.2% formic acid in 50% acetonitrile. The three elutions were pooled, and vacuum-centrifuged to dry. Samples were maintained at −20 °C until analysis[79].

Immobilized Metal Affinity Chromatography

115 µg of each sample was subjected to phosphopeptide enrichment. Enrichment was performed on a Bravo robot (Agilent Technologies) using AssayMAP Fe(III)-NTA, 5 µl cartridges (Agilent Technologies), according to the manufacturer's instructions. In brief, cartridges were primed and equilibrated with 50 µl of buffer A (99.9% ACN/0.1% TFA) and 100 µl of buffer C (80% ACN/19.9% H2O/0.1% TFA), followed by sample loading in 100 µl of buffer C at 5 µl/min. Phosphopeptides were eluted with 120 µl of buffer B (99% H2O/1% NH3) at 5 µl/min. Next, 3µl of formic acid was added to each sample for acidification. Prior to LC–MS analysis, all samples were concentrated to a volume of 15 µl[79].

Liquid chromatography

ULC/MS grade solvents were used for all chromatographic steps. Each sample was loaded using a split-less nano-Ultra Performance Liquid Chromatography column (10 kpsi nanoAcquity; Waters, Milford, MA, USA). The mobile phases were: A) H2O + 0.1% formic acid and B) acetonitrile + 0.1% formic acid. Desalting of the samples was performed online using a reversed-phase Symmetry C18 trapping column (180 µm internal diameter, 20 mm length, 5 µm particle size; Waters). The peptides were then separated using a T3 HSS nano-column (75 µm internal diameter, 250 mm length, 1.8 µm particle size; Waters) at 0.35 µL/min. Peptides were eluted from the column into the mass spectrometer using the following gradient: 4% to 33% B (for the global proteomics) or 20% B (for the phosphoproteomics) during 155 min, then to 90% B during 5 min, maintained at 90% for 5 min, and then returned to initial conditions [79].

Mass Spectrometry

The nanoUPLC was coupled online through a nanoESI emitter (10 µm tip; New Objective; Woburn, MA, USA) to a quadrupole orbitrap mass spectrometer (Q Exactive HF, Thermo Scientific) using a FlexIon nanospray apparatus (Proxeon). Data were acquired in data dependent acquisition (DDA) mode, using a Top10 method. MS1 resolution was set to 120,000 (at 200 m/z), mass range of 375-1650 m/z, AGC of 3e6 and maximum injection time was set to 60 msec. MS2 resolution was set to 15,000, quadrupole isolation 1.7m/z, AGC of 1e5, dynamic exclusion of 45 sec and maximum injection time of 60 msec for the global proteomics and 150 msec for the phosphoproteomics[79].

Proteomics data processing

Raw data were processed with MaxQuant v1.6.6.0[80,81]. The data were searched with the Andromeda search engine against the Uniprot human proteome database appended with common lab protein contaminants and the following modifications: Carbamidomethylation of C was noted as a fixed modification, oxidation of M and protein N-terminal acetylation as variable ones. For the phospho-sites analysis, phosphorylation of S, T and Y were added as well. The rest of the parameters were kept at default except for the following:

min. peptide length was set to 6, label and LFQ min. ratio count were set to 1, match between runs and iBAQ calculation were enabled, and the protein quantification was done on the basis of unique peptides only. The LFQ intensities (Label-Free Quantification) were extracted and used for further calculations using Perseus v1.6.2.3[82]. Decoy hits were filtered out, as well as proteins that were identified on the basis of a modified peptide only. The data were further filtered to include only proteins with at least 3 valid values in at least one of the groups. Protein expression imputation was done with a random low range normal distribution. A Student's t-test, after logarithmic transformation, was used to identify significant differences across the biological replica. Fold changes were calculated based on the ratio of geometric means of the different compared groups. Phospho analysis was done using the phospho-sites table generated by Maxquant. The data were filtered as in the global analysis. The intensities were normalized by subtracting the median, and missing values were imputed by a low constant. Statistics were performed similarly as for protein expression. Significant changes in protein abundance and phosphorylation levels were visualized using the EnhancedVolcano R package. A site was considered as differentially phosphorylated if its phosphorylation level significantly changed compared to WT (FC > 1.5 or <-1.5, $p<0.05$). Protein sites were excluded when the protein level was significantly changed in the same direction as the phosphorylation level (FC >1.25 or <-1.25, $p<0.1$). The Metascape tool was used to define unique pathways that were significantly modified using the threshold mentioned above[36].

Statistical analysis

Statistical significance was determined with GraphPad Prism Version 9.0 using the tests indicated in each figure.

Table S1
Antibodies used in flow cytometry and western blot.

Name	Clone	Manufacturer
Flow cytometry		
CD45R/B220	RA3-6B2	Biolegend
CD38	90	eBioscience
CD95/FAS	Jo2	BD Biosciences
IgM	II/41	eBioscience
IgG1	RMG1-1	Biolegend
IgG2ab	X-57	Miltenyi Biotec
IgA	RMA-1	Biolegend
CD138	281-2	Biolegend
CD86	GL-1	Biolegend
Western blot		
Beta-Actin	D6A8	Cell Signaling Technology
DYRK1A	D30C10	Cell Signaling Technology
DYRK1A	7D10	Abnova
MSH6	OTI5D1	Origene
Thiophosphate ester	51-8	Abcam
HRP anti mouse IgG	NXA931	Cytiva
HRP anti rabbit	NA934	Cytiva

1. Plotkin, S. A. Correlates of protection induced by vaccination. *Clin. Vaccine Immunol.* **17**, 1055–1065 (2010).
2. Laidlaw, B. J. & Ellebedy, A. H. The germinal centre B cell response to SARS-CoV-2. *Nat. Rev. Immunol.* **22**, 7–18 (2022).
3. Thomsen, A. R. *et al.* Cooperation of B cells and T cells is required for survival of mice infected with vesicular stomatitis virus. *Int. Immunol.* **9**, 1757–1766 (1997).
4. Wieland, A. & Ahmed, R. Fc Receptors in Antimicrobial Protection. *Curr. Top. Microbiol. Immunol.* **423**, 119–150 (2019).
5. DiLillo, D. J. & Ravetch, J. V. Fc-Receptor Interactions Regulate Both Cytotoxic and Immunomodulatory Therapeutic Antibody Effector Functions. *Cancer Immunology Research* vol. 3 704–713 (2015).
6. Webb, N. E., Bernshtein, B. & Alter, G. Tissues: the unexplored frontier of antibody mediated immunity. *Curr. Opin. Virol.* **47**, 52–67 (2021).
7. Lu, L. L., Suscovich, T. J., Fortune, S. M. & Alter, G. Beyond binding: antibody effector functions in infectious diseases. *Nat. Rev. Immunol.* **18**, 46–61 (2018).
8. Hajishengallis, G., Reis, E. S., Mastellos, D. C., Ricklin, D. & Lambris, J. D. Novel mechanisms and functions of complement. *Nat. Immunol.* **18**, 1288–1298 (2017).
9. Victora, G. D. & Nussenzweig, M. C. Germinal Centers. *Annual Review of Immunology* vol. 30 429–457 (2012).
10. Roco, J. A. *et al.* Class-Switch Recombination Occurs Infrequently in Germinal Centers. *Immunity* **51**, 337–350.e7 (2019).
11. Stavnezer, J., Guikema, J. E. J. & Schrader, C. E. Mechanism and Regulation of Class Switch Recombination. *Annual Review of Immunology* vol. 26 261–292 (2008).
12. Honjo, T., Kinoshita, K. & Muramatsu, M. Molecular mechanism of class switch recombination: linkage with somatic hypermutation. *Annu. Rev. Immunol.* **20**, 165–196 (2002).

13. Chaudhuri, J. & Alt, F. W. Class-switch recombination: interplay of transcription, DNA deamination and DNA repair. *Nat. Rev. Immunol.* **4**, 541–552 (2004).

14. Rush, J. S., Fugmann, S. D. & Schatz, D. G. Staggered AID- dependent DNA double strand breaks are the predominant DNA lesions targeted to Sμ in Ig class switch recombination. *Int. Immunol.* **16**, 549–557 (2004).

15. Zhang, X. *et al.* Fundamental roles of chromatin loop extrusion in antibody class switching. *Nature* **575**, 385–389 (2019).

16. Petersen-Mahrt, S. K., Harris, R. S. & Neuberger, M. S. AID mutates E. coli suggesting a DNA deamination mechanism for antibody diversification. *Nature* **418**, 99–103 (2002).

17. Feng, Y., Seija, N., Di Noia, J. M. & Martin, A. AID in Antibody Diversification: There and Back Again. *Trends Immunol.* **41**, 586–600 (2020).

18. Biram, A., Davidzohn, N. & Shulman, Z. T cell interactions with B cells during germinal center formation, a three- step model. *Immunol. Rev.* **288**, 37–48 (2019).

19. Gitlin, A. D., Shulman, Z. & Nussenzweig, M. C. Clonal selection in the germinal centre by regulated proliferation and hypermutation. *Nature* **509**, 637–640 (2014).

20. Xu, H. *et al.* Follicular T-helper cell recruitment governed by bystander B cells and ICOS-driven motility. *Nature* **496**, 523–527 (2013).

21. Rammohan, M. *et al.* The chromosome 21 kinase DYRK1A: emerging roles in cancer biology and potential as a therapeutic target. *Oncogene* **41**, 2003–2011 (2022).

22. Aranda, S., Laguna, A. & de la Luna, S. DYRK family of protein kinases: evolutionary relationships, biochemical properties, and functional roles. *FASEB J.* **25**, 449–462 (2011).

23. Arbones, M. L., Thomazeau, A., Nakano-Kobayashi, A., Hagiwara, M. & Delabar, J. M. DYRK1A and cognition: A lifelong relationship. *Pharmacol. Ther.* **194**, 199–221 (2019).

24. Malinge, S. *et al.* Increased dosage of the chromosome 21 ortholog Dyrk1a promotes megakaryoblastic leukemia in a murine model of Down syndrome. *J. Clin. Invest.* **122**, 948–962 (2012).

25. Thompson, B. J. *et al.* DYRK1A controls the transition from proliferation to quiescence during lymphoid development by destabilizing Cyclin D3. *J. Exp. Med.* **212**, 953–970 (2015).
26. Yabut, O., Domogauer, J. & D'Arcangelo, G. Dyrk1A overexpression inhibits proliferation and induces premature neuronal differentiation of neural progenitor cells. *J. Neurosci.* **30**, 4004–4014 (2010).
27. Soppa, U. *et al.* The Down syndrome-related protein kinase DYRK1A phosphorylates p27(Kip1) and Cyclin D1 and induces cell cycle exit and neuronal differentiation. *Cell Cycle* **13**, 2084–2100 (2014).
28. Chen, J.-Y., Lin, J.-R., Tsai, F.-C. & Meyer, T. Dosage of Dyrk1a shifts cells within a p21-cyclin D1 signaling map to control the decision to enter the cell cycle. *Mol. Cell* **52**, 87–100 (2013).
29. Becker, W. Emerging role of DYRK family protein kinases as regulators of protein stability in cell cycle control. *Cell Cycle* **11**, 3389–3394 (2012).
30. Soppa, U. & Becker, W. DYRK protein kinases. *Curr. Biol.* **25**, R488–9 (2015).
31. Liu, Q. *et al.* Tumor suppressor DYRK1A effects on proliferation and chemoresistance of AML cells by downregulating c-Myc. *PLoS One* **9**, e98853 (2014).
32. Dominguez-Sola, D. *et al.* The proto-oncogene MYC is required for selection in the germinal center and cyclic reentry. *Nat. Immunol.* **13**, 1083–1091 (2012).
33. Calado, D. P. *et al.* The cell-cycle regulator c-Myc is essential for the formation and maintenance of germinal centers. *Nat. Immunol.* **13**, 1092–1100 (2012).
34. Kwon, K. *et al.* Instructive role of the transcription factor E2A in early B lymphopoiesis and germinal center B cell development. *Immunity* **28**, 751–762 (2008).
35. Kracker, S. & Radbruch, A. Immunoglobulin class switching: in vitro induction and analysis. *Methods Mol. Biol.* **271**, 149–159 (2004).
36. Zhou, Y. *et al.* Metascape provides a biologist-oriented resource for the analysis of systems-level datasets. *Nat. Commun.* **10**, 1523 (2019).
37. Bhansali, R. S. *et al.* DYRK1A regulates B cell acute lymphoblastic leukemia through phosphorylation of FOXO1 and STAT3. *J. Clin. Invest.* **131**, (2021).

38. Christmann, M., Tomicic, M. T. & Kaina, B. Phosphorylation of mismatch repair proteins MSH2 and MSH6 affecting MutSalpha mismatch-binding activity. *Nucleic Acids Res.* **30**, 1959–1966 (2002).

39. Martomo, S. A., Yang, W. W. & Gearhart, P. J. A role for Msh6 but not Msh3 in somatic hypermutation and class switch recombination. *J. Exp. Med.* **200**, 61–68 (2004).

40. Li, Z. *et al.* The mismatch repair protein Msh6 influences the in vivo AID targeting to the Ig locus. *Immunity* **24**, 393–403 (2006).

41. Franklin, A. & Blanden, R. V. A/T-targeted somatic hypermutation: critique of the mainstream model. *Trends Biochem. Sci.* **31**, 252–258 (2006).

42. Alvarez, M., Altafaj, X., Aranda, S. & de la Luna, S. DYRK1A autophosphorylation on serine residue 520 modulates its kinase activity via 14-3-3 binding. *Mol. Biol. Cell* **18**, 1167–1178 (2007).

43. Muramatsu, M. *et al.* Specific expression of activation-induced cytidine deaminase (AID), a novel member of the RNA-editing deaminase family in germinal center B cells. *J. Biol. Chem.* **274**, 18470–18476 (1999).

44. Muramatsu, M. *et al.* Class switch recombination and hypermutation require activation-induced cytidine deaminase (AID), a potential RNA editing enzyme. *Cell* **102**, 553–563 (2000).

45. Crouch, E. E. *et al.* Regulation of AID expression in the immune response. *Journal of Experimental Medicine* vol. 204 1145–1156 (2007).

46. Tiller, T. *et al.* Efficient generation of monoclonal antibodies from single human B cells by single cell RT-PCR and expression vector cloning. *J. Immunol. Methods* **329**, 112–124 (2008).

47. Allen, D. *et al.* Timing, genetic requirements and functional consequences of somatic hypermutation during B-cell development. *Immunol. Rev.* **96**, 5–22 (1987).

48. Wiesendanger, M., Kneitz, B., Edelmann, W. & Scharff, M. D. Somatic Hypermutation in Muts Homologue (Msh)3-, Msh6-, and Msh3/Msh6-Deficient Mice Reveals a Role for the Msh2–Msh6 Heterodimer in Modulating the Base Substitution Pattern. *Journal of Experimental Medicine* vol. 191 579–584 (2000).

49. Recasens, A. *et al.* Global phosphoproteomics reveals DYRK1A regulates CDK1 activity in

glioblastoma cells. *Cell Death Discov* **7**, 81 (2021).

50. Allen, C. D. C., Okada, T. & Cyster, J. G. Germinal-center organization and cellular dynamics. *Immunity* **27**, 190–202 (2007).
51. Stark, G. R. & Taylor, W. R. Analyzing the G2/M Checkpoint. *Checkpoint Controls and Cancer* 051–082 doi:10.1385/1-59259-788-2:051.
52. Dimova, D. K. & Dyson, N. J. The E2F transcriptional network: old acquaintances with new faces. *Oncogene* **24**, 2810–2826 (2005).
53. Fishel, R. *et al.* The human mutator gene homolog MSH2 and its association with hereditary nonpolyposis colon cancer. *Cell* **77**, 1 p following 166 (1994).
54. Palombo, F. *et al.* GTBP, a 160-kilodalton protein essential for mismatch-binding activity in human cells. *Science* **268**, 1912–1914 (1995).
55. Stavnezer, J. & Schrader, C. E. Mismatch repair converts AID-instigated nicks to double-strand breaks for antibody class-switch recombination. *Trends Genet.* **22**, 23–28 (2006).
56. Masuda, K. *et al.* DNA polymerase θ contributes to the generation of C/G mutations during somatic hypermutation of Ig genes. *Proceedings of the National Academy of Sciences* vol. 102 13986–13991 (2005).
57. Zan, H. *et al.* The translesion DNA polymerase θ plays a dominant role in immunoglobulin gene somatic hypermutation. *EMBO J.* **24**, 3757–3769 (2005).
58. Li, Z., Woo, C. J., Iglesias-Ussel, M. D., Ronai, D. & Scharff, M. D. The generation of antibody diversity through somatic hypermutation and class switch recombination. *Genes Dev.* **18**, 1–11 (2004).
59. Li, Z. *et al.* Examination of Msh6- and Msh3-deficient mice in class switching reveals overlapping and distinct roles of MutS homologues in antibody diversification. *J. Exp. Med.* **200**, 47–59 (2004).
60. Martin, A. *et al.* Msh2 ATPase activity is essential for somatic hypermutation at a-T basepairs and for efficient class switch recombination. *J. Exp. Med.* **198**, 1171–1178 (2003).
61. Schrader, C. E., Edelmann, W., Kucherlapati, R. & Stavnezer, J. Reduced isotype switching in splenic B cells from mice deficient in mismatch repair enzymes. *J. Exp. Med.* **190**, 323–330 (1999).

62. Min, I. M. *et al.* The Smu tandem repeat region is critical for Ig isotype switching in the absence of Msh2. *Immunity* **19**, 515–524 (2003).

63. Schrader, C. E., Vardo, J. & Stavnezer, J. Mlh1 can function in antibody class switch recombination independently of Msh2. *J. Exp. Med.* **197**, 1377–1383 (2003).

64. Guo, X., Williams, J. G., Schug, T. T. & Li, X. DYRK1A and DYRK3 promote cell survival through phosphorylation and activation of SIRT1. *J. Biol. Chem.* **285**, 13223–13232 (2010).

65. Schwickert, T. A., Alabyev, B., Manser, T. & Nussenzweig, M. C. Germinal center reutilization by newly activated B cells. *J. Exp. Med.* **206**, 2907–2914 (2009).

66. Schwickert, T. A. *et al.* In vivo imaging of germinal centres reveals a dynamic open structure. *Nature* **446**, 83–87 (2007).

67. Liu, T. *et al.* DYRK1A inhibitors for disease therapy: Current status and perspectives. *Eur. J. Med. Chem.* **229**, 114062 (2022).

68. von Boehmer, L. *et al.* Sequencing and cloning of antigen-specific antibodies from mouse memory B cells. *Nat. Protoc.* **11**, 1908–1923 (2016).

69. Lefranc, M. P. *et al.* IMGT, the international ImMunoGeneTics database. *Nucleic Acids Res.* **27**, 209–212 (1999).

70. Ye, J., Ma, N., Madden, T. L. & Ostell, J. M. IgBLAST: an immunoglobulin variable domain sequence analysis tool. *Nucleic Acids Research* vol. 41 W34–W40 (2013).

71. Gupta, N. T. *et al.* Change-O: a toolkit for analyzing large-scale B cell immunoglobulin repertoire sequencing data. *Bioinformatics* **31**, 3356–3358 (2015).

72. Jaitin, D. A. *et al.* Massively parallel single-cell RNA-seq for marker-free decomposition of tissues into cell types. *Science* **343**, 776–779 (2014).

73. Keren-Shaul, H. *et al.* MARS-seq2.0: an experimental and analytical pipeline for indexed sorting combined with single-cell RNA sequencing. *Nat. Protoc.* **14**, 1841–1862 (2019).

74. Kohen, R. *et al.* UTAP: User-friendly Transcriptome Analysis Pipeline. *BMC Bioinformatics* **20**, 154 (2019).

75. Dobin, A. *et al.* STAR: ultrafast universal RNA-seq aligner. *Bioinformatics* **29**, 15–21 (2013).

76. Anders, S., Pyl, P. T. & Huber, W. HTSeq—a Python framework to work with high-throughput sequencing data. *Bioinformatics* **31**, 166–169 (2014).

77. Love, M. I., Huber, W. & Anders, S. Moderated estimation of fold change and dispersion for RNA-seq data with DESeq2. *Genome Biol.* **15**, 550 (2014).

78. Subramanian, A. *et al.* Gene set enrichment analysis: a knowledge-based approach for interpreting genome-wide expression profiles. *Proc. Natl. Acad. Sci. U. S. A.* **102**, 15545–15550 (2005).

79. Elinger, D., Gabashvili, A. & Levin, Y. Suspension Trapping (S-Trap) Is Compatible with Typical Protein Extraction Buffers and Detergents for Bottom-Up Proteomics. *J. Proteome Res.* **18**, 1441–1445 (2019).

80. Cox, J. & Mann, M. MaxQuant enables high peptide identification rates, individualized p.p.b.-range mass accuracies and proteome-wide protein quantification. *Nat. Biotechnol.* **26**, 1367–1372 (2008).

81. Cox, J. *et al.* Accurate proteome-wide label-free quantification by delayed normalization and maximal peptide ratio extraction, termed MaxLFQ. *Mol. Cell. Proteomics* **13**, 2513–2526 (2014).

82. Tyanova, S. *et al.* The Perseus computational platform for comprehensive analysis of (prote)omics data. *Nat. Methods* **13**, 731–740 (2016).